



HAL
open science

Optimal nonlinear Stokes–Mueller polarimetry for multi-photon processes

Xiaobo Li, Wei Liu, François Goudail, Shih-Chi Chen

► **To cite this version:**

Xiaobo Li, Wei Liu, François Goudail, Shih-Chi Chen. Optimal nonlinear Stokes–Mueller polarimetry for multi-photon processes. *Optics Letters*, 2022, 47 (13), pp.3287. 10.1364/OL.459457. hal-04492053

HAL Id: hal-04492053

<https://hal.science/hal-04492053>

Submitted on 6 Mar 2024

HAL is a multi-disciplinary open access archive for the deposit and dissemination of scientific research documents, whether they are published or not. The documents may come from teaching and research institutions in France or abroad, or from public or private research centers.

L'archive ouverte pluridisciplinaire **HAL**, est destinée au dépôt et à la diffusion de documents scientifiques de niveau recherche, publiés ou non, émanant des établissements d'enseignement et de recherche français ou étrangers, des laboratoires publics ou privés.

Optimal nonlinear Stokes-Mueller polarimetry for multi-photon processes

XIAOBO LI^{1,3}, WEI LIU¹, FRANÇOIS GOUDAIL^{2,4}, AND SHIH-CHI CHEN^{1,3,5}

¹Department of Mechanical and Automation Engineering, The Chinese University of Hong Kong, Shatin, N.T., Hong Kong SAR, China

²Université Paris-Saclay, Institut d'Optique Graduate School, CNRS, Laboratoire Charles Fabry, 91120, Palaiseau, France

³Centre for Perceptual and Interactive Intelligence, Shatin, N.T., Hong Kong SAR, China

⁴francois.goudail@institutoptique.fr

⁵scchen@mae.cuhk.edu.hk

Compiled March 6, 2024

Nonlinear polarimeters make it possible to measure the polarization properties of multi-photon processes and to characterize the nonlinear properties of materials. However, existing measurement strategies are not optimal and suffer from poor precision. In this Letter, we develop a rigorous optimization model adapted to nonlinear Stokes-Mueller polarimetry (SMP) in order to improve the estimation precision of the nonlinear Mueller matrix (MM) of two- and third-photon processes. Based on the model, we design measurement strategies that decrease the estimation variance of MM coefficients by about 58.2% for second-harmonic generation polarimetry and by 78.7% for third-harmonic generation polarimetry. The optimization model opens a door to improving the measurement precision of SMPs in nonlinear optics and can be readily applied to any multi-photon-based nonlinear polarimeters. © 2024 Optical Society of America

remains to be done for nonlinear polarimetry. This is the purpose of this Letter, where we determine the incoming and analysis polarization states (PS) that optimize the estimation precision of the nonlinear MM. Our results show that the proposed optimal solutions substantially improve estimation precision compared to conventional measurement strategies.

Let us first introduce a general principle of nonlinear SMP. Consider that several components of the incoming fundamental light having frequencies $\omega_1, \dots, \omega_n$ (e.g., $n = 2$ for SHG and $n = 3$ for THG) interact in a nonlinear material and give rise to output light at frequency ω_σ by a multi-photon process. The fundamental equation in Eq. (1) connects the PS of the outgoing radiation with the PSs of the incoming radiations.

$$\mathbf{s}'(\omega_\sigma) = \mathcal{M}^{(n)} \mathbf{S}^{(n)}(\omega_1, \dots, \omega_n) \quad (1)$$

where $\mathbf{s}'(\omega_\sigma)$ denotes the standard 4×1 SV describing the PS of the outgoing radiation at ω_σ (the symbol $'$ signifies the measured outgoing signal). The $(n+1)^2 \times 1$ -dimensional vector $\mathbf{S}^{(n)}(\omega_1, \dots, \omega_n)$ is the nonlinear SV describing the PSs of the interacting components of the incoming electric field.

Next, we introduce how $\mathbf{S}^{(n)}$ is defined. Without loss of generality, let us assume that the waves propagate along the Y direction. Their electric field vectors $\tilde{\mathbf{E}}^T = (\tilde{E}_X, \tilde{E}_Z^T)$, where the superscript T denotes transposition, lie in the orthogonal plane defined by the normal directions X and Z (see Fig. 1 (a)). The incoming electric fields induce a polarization P_i as:

$$P_i = \chi_{ijk \dots m}^{(n)} \tilde{E}_i \tilde{E}_j \dots \tilde{E}_m = \chi_{iA}^{(n)} \Psi_A^{(n)} \quad (2)$$

where $\chi^{(n)}$ denotes the n^{th} order nonlinear susceptibility tensor of a material, and (Einstein) summation is assumed over repeated indices (i.e., A). The index $i \in \{X, Z\}$ denotes the polarization direction for the outgoing radiation and the remaining indices j, k, \dots, m are polarization directions for the incoming electric fields. Moreover, $\Psi_A^{(n)}$ is the A^{th} element of the state function $\Psi^{(n)}$ of the incident electric field, and is expressed by Eq. (3).

$$\Psi^{(n)}(\omega_1, \omega_2, \dots, \omega_n) = \left(\psi_1^{(n)}, \psi_2^{(n)}, \dots, \psi_{n+1}^{(n)} \right)^T \quad (3)$$

As an example, let us assume that the considered nonlinear phenomenon is SHG, which is a two-photon process highly

1 <http://dx.doi.org/10.1364/ao.XX.XXXXXX>

2
3
4 The molecular organization and symmetry of materials can be
5 probed by polarization measurements of nonlinear multi-photon
6 processes occurring in assemblies of oriented molecules, such
7 as second-harmonic generation (SHG), third-harmonic gener-
8 ation (THG), coherent anti-Stokes Raman scattering (CARS),
9 etc. [1–3]. Nonlinear polarimetry differs from traditional linear
10 polarimetry since it involves higher-order polarization param-
11 eters, e.g., Stokes vector (SV) and Mueller matrix (MM), making
12 measurements more complex but also richer [4–6]. However,
13 polarization-dependent multi-photon processes always suffer
14 from poor signal-to-noise ratio (SNR), due to insufficient excita-
15 tion or conversion efficiency and to the presence of extra polariz-
16 ing elements. Of course, effective solutions may focus on enhanc-
17 ing the signal power and improving the excitation/conversion
18 efficiency [7]. However, it is also of prime importance to design
19 measurement strategies that get the most out of the incoming
20 signal and reduce corruption by noise. Much effort has been
21 made to design optimal measurement strategies in traditional
22 linear Stokes-Mueller polarimetry (SMP) [8–11]. A similar work

sensitive to the structure of ordered aggregates. In this case, one has $n = 2$, $\omega_1 = \omega_2 = \omega$, and $\omega_\delta = 2\omega$ in Eq. (1). The state function is $\Psi^{(2)} = (\tilde{E}_X^2, \tilde{E}_Z^2, 2\tilde{E}_X\tilde{E}_Z)^T$: it has $n + 1 = 3$ elements and the indices A in Eq. (2) belong in the set $\{X, Z, XZ\}$ [3, 12]. Let us define, the dyad product (coherency matrix) $\mathcal{C}^{(n)} = \langle \Psi^{(n)} \cdot \Psi^{(n)\dagger} \rangle$, where \dagger denotes the Hermitian conjugate. In the same way as the standard SV is defined from the coherency matrix of the Jones vector [13], each element of the nonlinear SV $\mathbf{S}^{(n)}$ can be defined from $\mathcal{C}^{(n)}$ as:

$$\mathbf{S}_N^{(n)} = \text{Tr}(\mathcal{C}^{(n)}\lambda_A^{(n)}) = \Psi^\dagger \lambda_A^{(n)} \Psi, \quad (4)$$

where $N = 0, 1, \dots, (n+1)^2 - 1$, and λ_A denotes the $(n+1) \times (n+1)$ dimensional Gell-Mann matrices, which are hermitian and obey the orthogonality relation $\text{Tr}(\lambda_i \lambda_j) = 2\delta_{ij}$ [14]. For SHG, the nonlinear SV has the following expression in Eq. (5) [3].

$$\mathbf{S}^{(2)} = \begin{pmatrix} \sqrt{\frac{2}{3}} (\tilde{E}_X^2 \tilde{E}_X^{*2} + \tilde{E}_Z^2 \tilde{E}_Z^{*2} + 4\tilde{E}_X \tilde{E}_Z \tilde{E}_X^* \tilde{E}_Z^*) \\ \sqrt{\frac{1}{3}} (\tilde{E}_X^2 \tilde{E}_X^{*2} + \tilde{E}_Z^2 \tilde{E}_Z^{*2} - 8\tilde{E}_X \tilde{E}_Z \tilde{E}_X^* \tilde{E}_Z^*) \\ \tilde{E}_X^2 \tilde{E}_X^{*2} - \tilde{E}_Z^2 \tilde{E}_Z^{*2} \\ \tilde{E}_X^2 \tilde{E}_Z^{*2} + \tilde{E}_Z^2 \tilde{E}_X^{*2} \\ 2(\tilde{E}_X^2 \tilde{E}_X^* \tilde{E}_Z + \tilde{E}_X \tilde{E}_Z \tilde{E}_Z^{*2}) \\ 2(\tilde{E}_X^2 \tilde{E}_X^* \tilde{E}_Z + \tilde{E}_X \tilde{E}_Z \tilde{E}_Z^{*2}) \\ (\tilde{E}_X^2 \tilde{E}_Z^{*2} - \tilde{E}_Z^2 \tilde{E}_X^{*2}) i \\ 2(\tilde{E}_X^2 \tilde{E}_X^* \tilde{E}_Z - \tilde{E}_X \tilde{E}_Z \tilde{E}_Z^{*2}) i \\ 2(\tilde{E}_X^2 \tilde{E}_X^* \tilde{E}_Z - \tilde{E}_X \tilde{E}_Z \tilde{E}_Z^{*2}) i \end{pmatrix} = \begin{pmatrix} \sqrt{\frac{1}{6}} (3s_0^2 - s_1^2) \\ \sqrt{\frac{1}{12}} (5s_1^2 - 3s_0^2) \\ -s_0 s_1 \\ \frac{1}{2} (s_2^2 - s_3^2) \\ s_2 (s_1 + s_0) \\ -s_2 (s_1 - s_0) \\ -s_2 s_3 \\ s_3 (s_1 + s_0) \\ s_3 (s_1 - s_0) \end{pmatrix} \quad (5)$$

The last term in Eq. (5) expresses the nonlinear SV as a function of the standard Stokes vector of the fundamental incident light illuminating the material, whose elements are defined as $s_t = \text{Tr}(\tilde{\mathbf{E}}\tilde{\mathbf{E}}^\dagger \tau_t)$, $t \in [0, 3]$, where τ_t are Pauli matrices, so that [13]:

$$\mathbf{s} = \begin{pmatrix} s_0 \\ s_1 \\ s_2 \\ s_3 \end{pmatrix} = \begin{pmatrix} \tilde{E}_Z \tilde{E}_Z^* + \tilde{E}_X \tilde{E}_X^* \\ \tilde{E}_Z \tilde{E}_Z^* - \tilde{E}_X \tilde{E}_X^* \\ \tilde{E}_Z \tilde{E}_X^* + \tilde{E}_X \tilde{E}_Z^* \\ (\tilde{E}_Z \tilde{E}_X - \tilde{E}_X \tilde{E}_Z) i \end{pmatrix} \quad (6)$$

Finally, we calculate the n^{th} order nonlinear MM $\mathcal{M}^{(n)}$, which depends on the $\chi^{(n)}$ of the material, by the expression in Eq. (7). $\mathcal{M}^{(n)}$ characterizes the nonlinear properties of materials and its measurement can reveal, for example, the organization of protein structures within various biological tissues [14].

$$\mathcal{M}_{iA}^{(n)} = \frac{1}{2} \text{Tr}(\tau_i \chi^{(n)} \lambda_A \chi^{(n)\dagger}) \quad (7)$$

Our purpose in this Letter is to find the polarimeter configuration that maximizes the estimation precision of $\mathcal{M}^{(n)}$. In practice, the elements of $\mathcal{M}^{(n)}$ can be estimated by measuring the outgoing SVs, which are generated by various PSs of the fundamental light illuminating the material. Figure 1 (a) displays the graphical representation of the \mathbf{S} of the incoming fundamental light and the \mathbf{s}' of the output light generated by a multi-photon process. Figure 1 (b) presents a typical nonlinear polarimeter. The fundamental PS is prepared by a PS generator (PSG), while the nonlinear signal is analyzed by passing it through a PS analyzer (PSA). The PSG and PSA can be constructed by using a linear polarizer (P) and a quarter-wave plate (QWP) oriented at desired angles [3]. Notably, when using a polarized laser as the source, the optical elements in PSG can be replaced with a QWP and a half-wave plate [4].

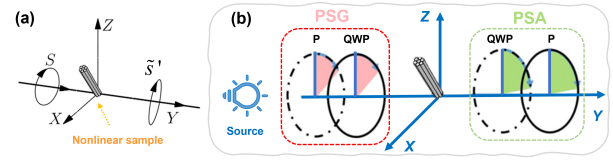


Fig. 1. (a) Graphical representations of the incoming \mathbf{S} and outgoing \mathbf{s}' PSs. (b) Nonlinear polarimeter.

In this section, we introduce the estimation model of MM based on the intensity measurements. Each column \mathbf{g}_p ($p \in [1, N_G]$, where N_G denotes the column number of \mathcal{G}) of PSG's measurement matrix \mathcal{G} is one of the standard SVs used to illuminate samples. The dimension of \mathcal{G} is thus $4 \times N_G$. Notably, each standard SV, i.e., \mathbf{g}_p , corresponds a nonlinear SV i.e., $\mathbf{S}_p^{(n)}$ (see, for example in the case of SHG, the last term of Eq. (5)). These generalized SVs $\mathbf{S}_p^{(n)}$ form a $(n+1)^2 \times 4$ matrix denoted $\mathcal{S}^{(n)}$. Similarly, each column of the measurement matrix \mathcal{T} of the PSA is one of the standard SVs \mathbf{t}_q ($q \in [1, N_T]$, where N_T denotes the column number of \mathcal{T}) used to analyze the output light. As in standard polarimeters, several intensity measurements are performed by illuminating the sample with a \mathbf{g}_p belonging to the matrix \mathcal{G} (corresponding to the $\mathbf{S}_p^{(n)}$ belonging to $\mathcal{S}^{(n)}$) and analyzing it with a \mathbf{t}_q belonging to \mathcal{T} . The expression of the measured intensity is:

$$i_{pq} = \mathbf{t}_q^T \mathcal{M}^{(n)} \mathbf{S}_p^{(n)}. \quad (8)$$

The values i_{pq} form a $N_G \times N_T$ matrix \mathcal{I} , and Eq. (8) is equivalent to the following relation:

$$\mathcal{I} = \mathcal{T}^T \mathcal{M}^{(n)} \mathcal{S}^{(n)}, \quad (9)$$

The matrix $\mathcal{M}^{(n)}$ is obtained by inverting this relation:

$$\mathcal{M}^{(n)} = (\mathcal{T}^{-1})^T \mathcal{I} [\mathcal{S}^{(n)}]^{-1} \quad (10)$$

Of course, for this inversion to be possible, the matrices \mathcal{G} and \mathcal{T} must be invertible. Hence, at least 4 analysis vectors have to be used (so that \mathcal{T} is square of dimension 4×4) and $(n+1)^2$ illumination vectors have to be used (so that \mathcal{S} is square of dimension $(n+1)^2 \times (n+1)^2$). Notably, it is of course possible to use more analysis and illumination vectors; in this case, the inversion in Eq. (10) must be replaced by the Moore-Penrose pseudo-inversion [15]. To facilitate the discussion, Eq. (10) can be rewritten as a vector-matrix product, as shown in Eq. (11).

$$\hat{\mathcal{M}}^{(n)} = \mathcal{K}^{-1} \mathbf{I} \quad (11)$$

where $\mathcal{K} = \mathcal{T}^T \otimes \mathcal{S}^{(n)}$, \otimes denotes the Kronecker product, and \mathbf{I} denotes the $4(n+1)^2 \times 1$ intensity vector obtained by stacking the elements of \mathcal{I} in Eq. (9).

Since the intensity acquisitions are always corrupted by noise, the estimate $\hat{\mathcal{M}}^{(n)}$ departs from the true value of $\mathcal{M}^{(n)}$. One of the mostly used performance criterion to characterize the estimation precision of polarimeters is the Equally Weighted Variance (EWV), which is defined by [11, 16]:

$$\text{EWV}_{\mathcal{K}} = \text{trace} \left[(\mathcal{K}^T \mathcal{K})^{-1} \right] = \text{trace} [D_{\mathcal{T}}] \times \text{trace} [D_{\mathcal{S}^{(n)}}] \quad (12)$$

where $D_U = (U^T U)^{-1}$ and $U = \{\mathcal{T}, \mathcal{S}^{(n)}\}$. In consequence:

$$\text{EWV}_{\mathcal{K}} = \text{EWV}_{\mathcal{T}} \times \text{EWV}_{\mathcal{S}^{(n)}} \quad (13)$$

Table 1. (α , ϵ) values for the common (Com.) and optimal (Opt.) configurations.

	α/ϵ ($^\circ$)
Com.	0/0, 90/0, 45/0, -45/0, 0/45, 0/-45, -22.5/0, 90/22.5, 45/-22.5
Opt.	120.3/166.4, 159.2/164.3, 45.0/177.2, 80.9/174.8, 61.5/71.6, 99.9/86.6, 41.7/32.5, 50.7/142.1, 17.8/70.8

As in the case of standard Mueller polarimetry, the goal of polarimeter optimization is to maximize $\text{EWW}_{\mathcal{K}}$, which, according to Eq. (13), amounts to find the analysis states of the PSA that maximize $\text{EWW}_{\mathcal{T}}$, and the illumination states of the PSG that maximize $\text{EWW}_{\mathcal{S}}$. It has been shown in conventional linear SMP that the optimal PSA matrix \mathcal{T} has regular tetrahedron structure when the minimal number of analysis states (i.e., 4) is used [10], and, more generally, a platonic polyhedron (PP) structure when an arbitrary number of illumination state is used [8]. In contrast, the optimization of the PSG is different from traditional polarimeters, since one has to minimize $\text{EWW}_{\mathcal{S}^{(n)}}$, that is, to solve the following optimization problem:

$$(\alpha^{opt}, \epsilon^{opt}) = \arg \min_{\alpha, \epsilon} \text{EWW}_{\mathcal{S}^{(n)}}. \quad (14)$$

where α and ϵ are $(n+1)^2 \times 1$ vectors representing, respectively, the azimuth and the ellipticity of SVs composing \mathcal{G} . The optimal solution of Eq. (14) is obviously different from that of

$$(\alpha^{opt}, \epsilon^{opt}) = \arg \min_{\alpha, \epsilon} \text{EWW}_{\mathcal{G}}, \quad (15)$$

because of the nonlinear relationship between the elements of \mathcal{S} and those of $\mathcal{S}^{(n)}$. Indeed, the optimal solutions of Eq. (15), which correspond to traditional PSG optimization in linear SMP, form a PP structure on the Poincaré sphere [8]. However, these solutions may not correspond to the minimization of $\text{EWW}_{\mathcal{S}}$. In the following, we will determine the optimal configurations for nonlinear SMPs of two- and three-photon processes, and evaluate the gain in performance compared to PSGs based on PP structure and common strategy [12].

Let us first consider the SMP for SHG. The expression of the nonlinear SV as a function of the standard SV of the fundamental illumination has been given in Eq. (5). In this case, $\mathcal{M}^{(2)}$ is a 4×9 matrix, and consequently, at least 36 intensity measurements are needed to obtain its 36 Mueller elements. Thus, the PSG has to generate nine different PSs, that is, \mathcal{G} is a 9×4 matrix, while the PSA generates four PSs and corresponds to a 4×4 matrix \mathcal{T} . The optimal PP structure for \mathcal{G} leads to a minimal value of $\text{EWW}_{\mathcal{G}} = 1.11$, but to $\text{EWW}_{\mathcal{S}^{(2)}} = 92.1$, which is too large and indicates that this solution is not a good choice. On the other hand, the most commonly chosen PSs in SHG polarimetry are shown in the first row of Table 1 [12]. They are slightly non optimal with respect to standard polarimetry, since $\text{EWW}_{\mathcal{G}} = 1.18$, but they are more favorable for SHG polarimetry since $\text{EWW}_{\mathcal{S}^{(2)}} = 16.7$. However, this solution has no reason to be optimal for SHG polarimetry. The optimal solution has to be found by solving the problem in Eq. (14).

To perform optimization searches for the problem in Eq. (14), one must note that the 18 parameters related to the 9 PSs of PSG need to be optimized simultaneously. Moreover, as the optimization criterion is nonconvex, it has numerous local minima. It is thus necessary to use an effective algorithm robust to

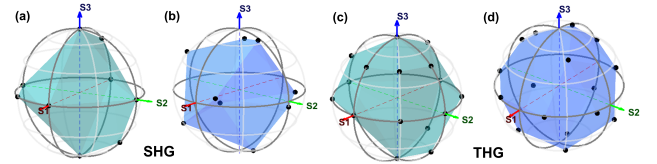
the presence of local minima. After comparing different algorithms, we have chosen to use the "inter point" method combined with "Multi-Starting points" [17, 18]. Simultaneous optimization of 18 PSG parameters (α^{opt} , ϵ^{opt}) yields the result presented in the second row of Table 1. The obtained criterion value is $\text{EWW}_{\mathcal{S}^{(2)}} = 6.98$. Compared with the common configuration of SHG polarimetry (first row of Table 1), the value of $\text{EWW}_{\mathcal{S}^{(2)}}$ is reduced by about 58.2%, while compared with the PP structure (See Supplement 1, Note 1, for more information.), it reduced by about 92.4%. We also calculate the estimation standard deviation (STD) of each element of $\mathcal{M}^{(2)}$ by using the two configurations in Table 1, that we put in two 4×9 matrices $\text{STD}[\mathcal{M}]_{com}$ and $\text{STD}[\mathcal{M}]_{opt}$: the expressions are shown in the Supplement 1, Note 2. To evaluate the improvement in estimation precision of each Mueller element, we calculate the STD ratio between the two configurations by the expression in Eq. (16).

$$\text{STD}_R = \frac{\text{STD}[\mathcal{M}]_{com}}{\text{STD}[\mathcal{M}]_{opt}}, \quad (16)$$

We have noticed that each row of the matrix STD_R has the same values, namely,

$$\text{STD}_R(i,:) = [1.2, 0.7, 1.4, 0.6, 3.0, 4.1, 4.4, 3.1, 2.2], \quad (17)$$

where $i \in [1, 4]$. It shows that, with the optimal configuration, the estimation STD values of most Mueller elements (except the 2nd and 4th columns of the nonlinear MM) are significantly reduced, especially the 5th, 6th, 7th and 8th columns. Figure 2 (a) and (b) display the SVs of the PSG matrices \mathcal{G} of the commonly used and optimal configurations on the Poincaré sphere. From Fig. 2, we may observe that, although the solution with PP structure is not optimal, the found optimal solution of Eq. (14) has a structure similar to a regular polyhedron. This is because the target matrix $\mathcal{S}^{(2)}$ is related to the fundamental incoming SV, i.e., the eigenvectors \mathcal{G} of PSG, in a nonlinear way.

**Fig. 2.** PSs of PSG located on the Poincaré sphere with the commonly used (a, c) and optimal (b, d) configurations.

The optimization model above can be also applied to two other two-photon processes, namely, sum-frequency generation (SFG) and difference frequency generation (DFG). Their nonlinear SV (i.e., $\mathbf{S}^{(2)}$) are also comprised of nine components and the related state functions are expressed in Eq. (18).

$$\begin{pmatrix} \tilde{E}_{X,\omega_1} \tilde{E}_{X,\omega_2}, \tilde{E}_{Z,\omega_1} \tilde{E}_{Z,\omega_2}, \tilde{E}_{X,\omega_1} \tilde{E}_{Z,\omega_2} + \tilde{E}_{X,\omega_2} \tilde{E}_{Z,\omega_1} \end{pmatrix}^T, \quad (18)$$

$$\begin{pmatrix} \tilde{E}_{X,\omega_1}, \tilde{E}_{X,\omega_2}^*, \tilde{E}_{Z,\omega_1}, \tilde{E}_{Z,\omega_2}^*, \tilde{E}_{X,\omega_1} \tilde{E}_{Z,\omega_2}^* + \tilde{E}_{X,\omega_2} \tilde{E}_{Z,\omega_1}^* \end{pmatrix}^T$$

Using Eq. (4) and Eq. (18), one can obtain the expressions of $\mathbf{S}^{(2)}$, which are listed in Supplement 1, Note 3. Subsequently, we can obtain the optimal configurations by solving the same problem in Eq. (14). Interestingly, we find that, in the case of SFG, optimal configurations for the two fundamental illumination beams (with frequency ω_1 and ω_2) are identical to that of SHG (i.e., the second row of Table 1). This is because the nonlinear SV of SFG (as shown in Eq. (S-3)) is similar to that of SHG (as

shown in Eq. (5) and satisfies $S_{(\omega_1, \omega_2)} = S_{(\omega_2, \omega_1)}$, which means that the two beams share the same PSG optimal structure.

Let us now consider the SMP of three photon processes, i.e., $n = 3$ in Eq. (1). Such processes (e.g., THG and CARS) are based on incoming radiations with three potentially distinct frequencies and result in an outgoing radiation determined by a third-order susceptibility tensor, i.e., $\chi^{(3)}$, of the material. As an example, we first consider the optimization of THG polarimetry. Polarimetric measurements of THG in crystalline material, ordered aggregates or isotropic media carry information related to the nonlinear optical properties and organization of the structure in a material [19, 20]. In this case, $\omega_i = \omega$, $i \in [1, 3]$, and $\omega_\delta = 3\omega$ in Eq. (1); and $\Psi^{(3)} = (\tilde{E}_X^3, \tilde{E}_Z^3, 3\tilde{E}_X^2\tilde{E}_Z, 3\tilde{E}_X\tilde{E}_Z^2)^T$ [1]. Subsequently, each element of the nonlinear SV is calculated by:

$$S_N^{(3)} = \text{Tr} \left(C^{(3)} \lambda_A^{(3)} \right) = \left[\Psi^{(3)} \right]^\dagger \lambda_A^{(3)} \Psi^{(3)}, \quad (19)$$

where $N = 0, 1, \dots, 15$, and $\lambda_A^{(3)}$ are 4×4 matrices [1]. Similar to SHG, one can obtain the expression of the nonlinear SV as a function of the illuminating standard SV [1, 19], which is shown in Eq. (20).

$$\mathbf{S} = \frac{1}{4} \begin{pmatrix} \sqrt{2}s_0 (5s_0^2 - 3s_1^2) \\ \sqrt{6} \left(-\frac{4}{3}s_0^3 + 3s_0^2s_1 + 2s_0s_1^2 - 3s_1^3 \right) \\ \sqrt{3} \left(-\frac{8}{3}s_0^3 - 3s_0^2s_1 + 4s_0s_1^2 + 3s_1^3 \right) \\ s_1 (3s_0^2 + s_1^2) \\ s_2 (s_2^2 - 3s_3^2) \\ 3(s_0 - s_1) (s_2^2 - s_3^2) \\ 9s_2 (s_2^2 + s_3^2) \\ 3s_2 (s_0 - s_1)^2 \\ 3s_2 (s_0 + s_1)^2 \\ 3(s_0 + s_1) (s_2^2 - s_3^2) \\ s_3 (3s_2^2 - s_3^2) \\ -6s_2s_3 (s_0 - s_1) \\ 9s_3 (s_2^2 + s_3^2) \\ -3s_3 (s_0 - s_1)^2 \\ 3s_3 (s_0 + s_1)^2 \\ 6s_2s_3 (s_0 + s_1) \end{pmatrix}. \quad (20)$$

The most commonly used PSs of the PSG in THG polarimetry are defined as $\alpha = (0^\circ, 90^\circ, 45^\circ, -45^\circ, 0^\circ, 0^\circ, -22.5^\circ, 90^\circ, 45^\circ, 22.5^\circ, 67.5^\circ, 22.5^\circ, 90^\circ, 45^\circ, 0^\circ, -22.5^\circ)$ and $\varepsilon = (0^\circ, 0^\circ, 0^\circ, 0^\circ, 45^\circ, -45^\circ, 0^\circ, 22.5^\circ, -22.5^\circ, 0^\circ, 0^\circ, 22.5^\circ, -22.5^\circ, 22.5^\circ, 22.5^\circ, 22.5^\circ)$. With this configuration, one has $\text{EWW}_S = 79.2$. By applying the same optimization approach as for SHG polarimetry, we can get the optimal solution of THG polarimetry, which results in $\text{EWW}_{S^{(3)}} = 16.9$. Compared with the most commonly chosen one, the value of EWW_S is reduced by about 78.7%. A similar visual comparison for THG polarimetry is shown in Figs. 2 (c) and (d). Besides, compared with the PP structure ($\text{EWW}_S = 22.5$), the EWW value reduced by about 24.9% (See Supplement 1, Note 1, for more information.) The optimization approach can be extended to other three-photon processes by redefining the state function $\Psi^{(3)}$

(e.g., $(\tilde{E}_{X,\omega_p}^2, \tilde{E}_{X,\omega_s}^*, \tilde{E}_{Z,\omega_p}^2, \tilde{E}_{Z,\omega_s}^*, 3\tilde{E}_{X,\omega_p}^2, \tilde{E}_{Z,\omega_s}^*, 3\tilde{E}_{Z,\omega_p}, \tilde{E}_{X,\omega_s}^*)^T$ for the CARS process, where ω_p and ω_s respectively denote the frequencies of the pump Stokes beams [21].)

All the results verify the necessity of optimization for nonlinear SMPs in improving the estimation precision. In addition, as the signal's SNR is inversely proportional to the EWV value, i.e., $\text{SNR} \propto 1/\text{EWV}$, optimal configurations increase the SNR values by about 1.4 and 3.7 times for SHG and THG, respectively. These improvements also present interesting opportunities for counteracting the adverse effects of the polarizing elements on signals's SNR and increasing the measurement precision.

In conclusion, we have developed an optimization model for nonlinear SMP setups. The estimation precision can be significantly increased by adopting the proposed optimized configuration, i.e., improve by 58.2% for SHG- and 78.7% for THG-polarimetry. The main perspectives of this work are experimental validation and to further extend to three-dimensional nonlinear SMPs [5, 6], which are of interest in both biological and physical contexts.

Funding. Centre for Perceptual and Interactive Intelligence Ltd under the Innovation and Technology Fund (A-CUHK-16-5-14); The Innovation Technology Commission (ITS/178/20FP).

Acknowledgments. The authors acknowledge Dr. Yu Zhang, University of Nottingham for fruitful discussions.

Disclosures. The authors declare no conflicts of interest.

Data availability. No data were generated or analyzed in the presented research.

Supplemental document. See Supplement 1 for supporting content.

REFERENCES

- M. Samim, S. Krouglov, and V. Barzda, Phys. Rev. A **93**, 033839 (2016).
- N. Mazumder, J. Qiu, M. R. Foreman, C. M. Romero, C. Hu, H. Tsai, P. Török, and F. J. Kao, Opt. Express **20**, 14090 (2012).
- M. Samim, S. Krouglov, and V. Barzda, JOSA B **32**, 451 (2015).
- Y. Shi, W. McClain, and R. Harris, Phys. Rev. A **49**, 1999 (1994).
- G. J. Simpson, The J. Phys. Chem. B **120**, 3281 (2016).
- S. Krouglov and V. Barzda, JOSA B **36**, 541 (2019).
- X. Qi, C. Du, and P. Liu, IEEE Transactions on Electron Devices **62**, 3399 (2015).
- M. R. Foreman, A. Favaro, and A. Aiello, Phys. Rev. Lett. **115**, 263901 (2015).
- X. Li, T. Liu, B. Huang, Z. Song, and H. Hu, Opt. Express **23**, 27690 (2015).
- F. Goudail, Opt. Lett. **34**, 647 (2009).
- X. Li, H. Hu, F. Goudail, and T. Liu, Opt. Express **27**, 31261 (2019).
- C. Okoro and K. C. Toussaint, J. Biomed. Opt. **21**, 016011 (2016).
- J. J. Gil and R. Ossikovski, Polarized light and the Mueller matrix approach (CRC press, 2017).
- C. J. Sheppard, M. Castello, and A. Diaspro, JOSA A **33**, 1938 (2016).
- X. Li, H. Hu, L. Wu, and T. Liu, Opt. Express **25**, 18872 (2017).
- G. Anna and F. Goudail, Opt. Express **20**, 21331 (2012).
- S. Boyd, S. P. Boyd, and L. Vandenberghe, Convex Optimization (Cambridge university press, 2004).
- X. Li, H. Hu, L. Wu, Y. Yu, and T. Liu, J. Quant. Spectrosc. Radiat. Transf. **231**, 22 (2019).
- C. Shaji, R. Ismail, S. Satyanarayana, and A. Sharan, J. Nonlinear Opt. Phys. & Mater. **26**, 1750040 (2017).
- M. Samim, S. Krouglov, and V. Barzda, Phys. Rev. A **93**, 013847 (2016).
- T. Würthwein, M. Brinkmann, T. Hellwig, and C. Fallnich, The J. Chem. Phys. **147**, 194201 (2017).